Coupled radiation-conduction heat transfer in layered composite scintillation ceramics

YUXUAN HONG[1], YANYAN BU[1,2*], XIANGFU WANG[1,3*]
[1]*College of Electronic and Optical Engineering & College of Microelectronics, Nanjing University of Posts and Telecommunications, Nanjing, 210046, People's Republic of China*
[2]*College of Science, Nanjing University of Posts and Telecommunications, Nanjing, 210046, People's Republic of China*
[3]*Anhui Province Key Laboratory of Environment-friendly Polymer Materials, Anhui University, Hefei, People's Republic of China*

The layered ceramic scintillator has become a new type of optical ceramic with high single crystal utilization and strong ability to discern pulse shape. However, there are few studies on the radiation-conduction heat transfer propagation and intensity change in the layered ceramic scintillator. Based on the layered composite ceramic GGAG/YAG, this paper reports a three-dimensional optical radiation transmission model solved by path divergence method. The coupled radiation-conduction heat transfer at various distances from GGAG ceramic to the YAG ceramic is calculated. It is found that this method can accurately and efficiently obtain heat transfer in composite scintillation ceramics. The radiation intensity decays exponentially with the distance after passing through the interface between the two layers of layered ceramics. The smaller the incident angle of radiation, the greater the radiation intensity. When the angle of incidence approaches 35 degrees, the curve begins to distort. When the radiation passes through the ceramic and enters the air, the radiation decays approximately linearly.

(Received September 20, 2021; accepted April 7, 2022)

Keywords: Radiation, Conduction, Heat transfer

1. Introduction

At present, layered composite ceramics have received extensive attention in the preparation of high temperature resistant and scintillator materials. In terms of thermal radiation transmission, some methods to make layered ceramics more resistant to fracture at high temperatures and to enhance the high temperature properties of ceramics have been proposed and applied to layered composite scintillating ceramics. For example, enhanced thermal shock response of Al_2O_3–graphite composites [1] and Roman crucibles with strong high temperature performance [2] and so on [3-6]. In terms of scintillation characteristics, composite ceramics have some advantages: stronger ability to discern pulse shape, higher single crystal utilization [7] and so on. It has broad application in medical imaging, especially cancer treatment [8]; ionization detection [9]; petroleum logging; astrophysics [10]; X-ray detection [11], etc. Typical layered composite ceramics are $Gd_3Al_3Ga_2O_{12}$, $Y_3Al_5O_{12}$, Eu:$(Y,Gd)_2O_3$, Ce:$(Lu,Tb)_3Al_5O_{12}$, Pr:Gd_2O_2S, SnF_2-SnO-P_2O_5 and so on. Among them, GGAG, YAG, Eu:$(Y,Gd)_2O_3$, Ce:$(Lu,Tb)_3Al_5O_{12}$, Pr:Gd_2O_2S can be used as ceramic scintillators. GGAG/YAG layered composite ceramics have been applied to improve the exploration of full-spectrum scintillation/luminescence ceramics preparation and spectra designation [12]. Few scholars have studied the coupled radiation transfer in the layered composite scintillator, however, because modern measuring instruments cannot measure the changes of radiation intensity in a single ceramic and at the interface of layered ceramics. Therefore, it is very necessary and important to study on the process of radiation conduction in composite scintillation ceramics.

In fact, radiation and heat conduction coexist in the process of light emission. If only radiation or only heat conduction is considered, the results of thermal analysis will be biased [13]. Therefore, the coupling effect of radiation and heat conduction needs to be considered simultaneously. In order to analyze and calculate the process of radiation conduction, it is necessary to establish a heat conduction model that simulates radiation process from one layer of medium to another layer and then to surrounding. At present, representative numerical solutions on radiative transmission problems are the zone method (ZM) proposed by Hottel and Cohen [14], the discrete coordinate method (DOM) proposed by Chandrasekhar [15], the spherical harmonic method (SHM) proposed by Jeans [16], and Ray tracing method (RTM) proposed by Tan [17]. Recently, some new methods have also been used in the field of radiative transfer. For example, the Monte Carlo ray tracing method by Zhang [18], a more

accurate time-integrated method by Julio [19] and the stochastic model by Banko [20]. However, in the layered composite scintillating ceramics, ZM has difficulty in handling complex boundary conditions due to the non-uniform area; DOM has a large error for the continuity of the radiation field; SHM does not consider coupling effects; RTM cannot handle interface effects. Therefore, this paper proposes a path divergence method (PDM) based on Boltzmann's equation and a general form of radiation transfer equation. This method has a wide range of applications and can deal with three-dimensional multilayer media coupling transmission problems.

2. Model and method

The path divergence method(PDM) is shown in Fig. 1. When calculating the radiation intensity $I(\lambda, p_M, \Psi)$ at any point M in any direction Ψ in the medium by this method, one just needs to know the intensity of any point N $I(\lambda, p_N, \Psi)$ that along the path in this direction from this point in the medium, all control bodies ΔV_i 's generalized source item size $B(\lambda, p, \Psi)$ on the path between these two points and the distance Δs_i that the radiation travels in these control bodies.

As we all know, in the theory describing the radiation transmission process of light in semi-transparent media, two different methods will be selected correspondingly according to the target feature size. When the target feature size is close to the incident wavelength, it is necessary to solve Maxwell's equations [21]. It is studied by the electromagnetic wave theory. When the characteristic size of the target is much larger than the incident wavelength, it can be studied by solving the transport theory of Boltzmann equation [22]. Since the characteristic size of the research object in this paper is much larger than the incident wavelength of the laser, the radiation transfer equation is solved.

The radiation transfer equation can be written as [23]:

$$\frac{n}{c}\frac{\partial I(\lambda,p,\Psi,t)}{\partial t} + n^2\frac{\partial}{\partial s}\left[\frac{I(\lambda,p,\Psi,t)}{n^2}\right] = -\beta I(\lambda,p,\Psi,t) + n^2\gamma I_s(\lambda,p,t) + \frac{\sigma_s}{4\pi}\int_0^{4\pi} I(\lambda,p,\Psi',t)\cdot\Phi(\Psi,\Psi')d\boldsymbol{\Psi}' \quad (1)$$

In the formula, n represents the refractive index of the medium; c_0 represents the speed of light in vacuum, [m/s]; $I(\lambda, p, \Psi, t)$, represents the radiation intensity at time t, position p, direction of Ψ, with the wavelength of λ, $[W/m^2 \cdot \mu m \cdot sr)]$; s is the distance in the direction of Ψ, [m]; β is the attenuation coefficient, [m^{-1}];γ is the absorption coefficient, [m^{-1}]; σ_s is the scattering coefficient, [m^{-1}]; $\Phi(\Psi, \Psi')$ means Ψ' direction incident, the size of the scattering phase function scattered along the Ψ direction; $\boldsymbol{\Psi}'$ represents the solid angle size in the Ψ' direction, [sr].

Because the speed of radiation propagation is much greater than the speed of temperature response, it is generally considered to be a steady-state radiation transmission problem [24], so the effect of time is not considered, and the steady-state radiation transfer equation is used to describe:

$$\frac{dI(\lambda,p,\Psi)}{ds} = -\beta I(\lambda,p,\Psi) + n^2\gamma I_s(\lambda,p) + \frac{\sigma_s}{4\pi}\int_0^{4\pi} I(\lambda,p,\Psi')\cdot\Phi(\Psi,\Psi')d\boldsymbol{\Psi}' \quad (2)$$

In the formula, the left side of the equal sign represents the change of radiation intensity within the micro-element ds; the three terms on the right are the attenuation terms of intensity from left to right, the enhancement term of radiation in the micro-element section itself and the enhancement term caused by scattering in other directions.

$$B(\lambda,p,\Psi) = n^2\gamma I_s(\lambda,p) + \frac{\sigma_s}{4\pi}\int_0^{4\pi} I(\lambda,p,\Psi')\cdot\Phi(\Psi,\Psi')d\boldsymbol{\Psi}' \quad (3)$$

Equation (2) can be transformed into equation (4).

$$\frac{dI(\lambda,p,\Psi)}{ds} = -\beta I(\lambda,p,\Psi) + B(\lambda,p,\Psi) \quad (4)$$

To solve (λ, p, Ψ) , transform equation (4) into equation (5).

$$\frac{d}{ds}\left[I(\lambda,p,\Psi)\cdot e^{\beta\cdot s}\right] = B(\lambda,p,\Psi)\cdot e^{\beta\cdot s} \quad (5)$$

Integrate both sides as follows:

$$\int_0^{\Delta s} d[I(\lambda,p,\Psi)\cdot e^{\beta\cdot s}] = \int_0^{\Delta s} B(\lambda,p,\Psi)\cdot e^{\beta\cdot s}ds \quad (6)$$

After integrating and simplifying the infinitesimal Δs, as shown in Fig. 1, we get:

$$I(\lambda,p_2,\Psi) = I(\lambda,p_1,\Psi)\cdot e^{-\beta\cdot\Delta s} + \frac{B(\lambda,p,\Psi)}{\beta\cdot\left[1-e^{-\beta\cdot\Delta s}\right]} \quad (7)$$

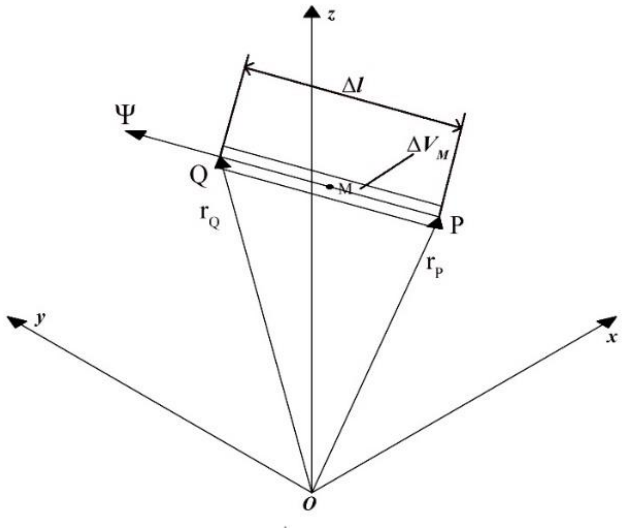

Fig. 1. Schematic diagram of path divergence method

According to the idea of this path element, for ceramics, the strength boundary condition in any direction on the boundary can be solved by the following formula:

$$I(\lambda,p,\Psi)=n^2\cdot\frac{\varepsilon(\lambda)}{\pi}\cdot\eta(\lambda,T)\cdot\sigma\cdot T^4(p)+\frac{1-\varepsilon(\lambda)}{\pi}\cdot \sum_{e\cdot\Psi'<0} I(\lambda,p,\Psi')\cdot|e\cdot\Psi'|\cdot\Delta\boldsymbol{\Psi}' \quad (8)$$

In the formula, n represents the refractive index of the medium; $\varepsilon(\lambda)$ represents the emissivity of the boundary at the wavelength λ; $\eta(\lambda,T)$ represents the wavelength λ, temperature T is the share of blackbody radiation in the total radiation, $[\mu m^{-1}]$; σ is Boltzmann's constant $\sigma=5.6703\times10^{-8}[W/(m^2\cdot K^4)]$; $T(p)$ represents the temperature at the boundary, [K]; e represents the normal unit vector at the boundary; $\boldsymbol{\Delta\Psi}'$ represents the solid angle in the direction of Ψ', [sr].

In Fig. 2, for the interface of the medium, the incident radiation intensity is I_0, the refractive index of medium 1 is n_1, the refractive index of medium 2 is n_2, the refractive index of medium 3 is n_3, the incident angle is θ and the refraction angle is φ.

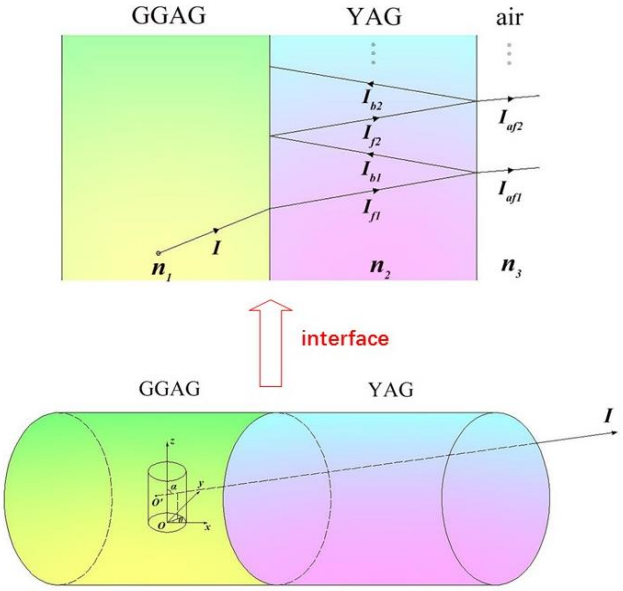

Fig. 2. Physical schematic diagram of the model (color online)

When the angle θ is less than the critical angle θ_0, the reflectivity from the left medium to the right medium can be calculated by the following formula [25]:

$$\rho_{12}(\theta)=\frac{1}{2}\left[\left(\frac{cos\theta\cdot n_2-cos\varphi\cdot n_1}{cos\theta\cdot n_2+cos\varphi\cdot n_1}\right)^2+\left(\frac{cos\theta\cdot n_1-cos\varphi\cdot n_2}{cos\theta\cdot n_1+cos\varphi\cdot n_2}\right)^2\right] \quad (9)$$

Among them, according to Snell's law:

$$\frac{sin\theta}{sin\varphi}=\frac{n_2}{n_1} \quad (10)$$

The light intensity $I(x,\theta)$ at the interface can be divided into refracted light intensity $I_f(x,\theta)$ and reflected reverse light intensity $I_b(x,\theta)$, which are represented by the following formulas considering the effect of refraction and reflection:

$$I_f(x,\theta)=I_0\cdot(1-\rho_{12})\cdot\frac{{n_2}^2}{{n_1}^2}\cdot e^{-\frac{\beta x}{cos\varphi}} \quad (11)$$

$$I_b(x,\theta)=I_0\cdot(1-\rho_{12})\cdot\rho_{23}\cdot\frac{{n_2}^2}{{n_1}^2}\cdot e^{-\frac{\beta(2L-x)}{cos\varphi}} \quad (12)$$

After two reflections, the forward radiation intensity I_{f2} projected on the position x is:

$$I_{f2}(x,\theta)=I_0\cdot(1-\rho_{12})\cdot\rho_{23}\cdot\rho_{21}\cdot\frac{{n_2}^2}{{n_1}^2}\cdot e^{-\frac{\beta(2L+x)}{cos\varphi}} \quad (13)$$

After three reflections, the backward radiation intensity I_{b2} projected on the position x is:

$$I_{f2}(x,\theta)=I_0\cdot(1-\rho_{12})\cdot{\rho^2}_{23}\cdot\rho_{21}\cdot\frac{{n_2}^2}{{n_1}^2}\cdot e^{-\frac{\beta(4L-x)}{cos\varphi}} \quad (14)$$

By analogy, the forward and backward radiation intensities respectively form a series of equal ratios, and the common ratio is $\rho_{23} \cdot \rho_{21} \cdot e^{-\frac{2\beta L}{cos\varphi}}$.

According to the summation formula of the proportional sequence, it can be obtained that after infinite reflections, the total radiation intensity I_{tot} at the x position in the medium is:

$$I_{tot}(x,\theta) = \frac{I_0(1-\rho_{12}) \cdot \frac{{n_2}^2}{{n_1}^2} \cdot [e^{-\frac{\beta x}{cos\varphi}} + \rho_{23} \cdot e^{-\frac{\beta(2L-x)}{cos\varphi}}]}{1 - \rho_{23} \cdot \rho_{21} \cdot e^{-\frac{2\beta L}{cos\varphi}}} \tag{15}$$

Generally speaking, since the propagation speed of radiation energy is much greater than the speed of temperature response, it can be considered that the radiation energy has reached equilibrium within the temperature relaxation time. That is, this is a steady-state radiation transmission problem. In addition, assuming that the deduced boundary conditions in the above model are all semi-transparent, since the Fresnel interface is more difficult to handle than the diffuse interface, only the case when all the interfaces are Fresnel interfaces is deduced here.

As shown in Fig. 2, take a cylinder with a radius of 0.5 m and a height of H=20 m in ceramic 1, and the refractive index n=0.77. Set the temperature field of the entire medium as T=2000 K, and the attenuation coefficient β = 2 m^{-1}.

3. Results and discussion

The absorption coefficient of GGAG and YAG is 0.11 cm^{-2} and 0.002 cm^{-2} respectively [26-27]. Fig. 3(a) shows the calculation result of the corresponding radiation intensity when the scattering albedo ω is 0.2, 0.5 and 0.8 respectively, the zenith angle α changed from 10° to 170° with the circumferential angle $\theta = 45°$. It can be seen that the radiation intensity in the left and right directions of the zenith angle $\alpha = 90°$ is symmetrical. Fig. 3 (b) shows the calculation result of the corresponding radiation intensity when the scattering albedo ω is 0.2, 0.5 and 0.8 respectively, the circumference angle θ changed from 15° to 75° with the zenith angle $\alpha = 90°$. It can be seen that the radiation intensity in the left and right directions of the circumferential angle $\theta = 45°$ is symmetrical. Observing Fig. 2, it can be seen that the radiation intensity passes through the center of the cylinder when the circumferential angle $\theta = 45°$ and the zenith angle $\alpha = 90°$. Fig. 3(c) shows the schematic of detection rays with different azimuthal angles. Fig. 3(d) shows the radiation intensity changes in the directions of $\theta = 30°, 45°, 60°, 75°, 90°$ starting from the point o' when considering the uneven temperature field and the attenuation coefficient field. Among them, the scattering albedo $\omega = 0.5$, the zenith angle $\alpha = 90°$, the horizontal distance from o' point is r, and the temperature field and attenuation coefficient field at the height z are given by equations (16) and (17).

$$T(r,z) = -\frac{2600}{17} \cdot (z-20) \cdot (0.5 - 3r^2 + 2r^3) + 800 \tag{16}$$

$$\beta(r,z) = -0.15 \cdot (z-20) \cdot (0.5 - 3r^2 + 2r^3) + 0.8 \tag{17}$$

Through the above calculation, the radiation intensity distribution in each direction in ceramic 1 (GGAG) can be obtained. This is the first step to solve the problem of light passing through the layered ceramic scintillator. Next, we solve the interface and the distribution after radiation passing through the interface.

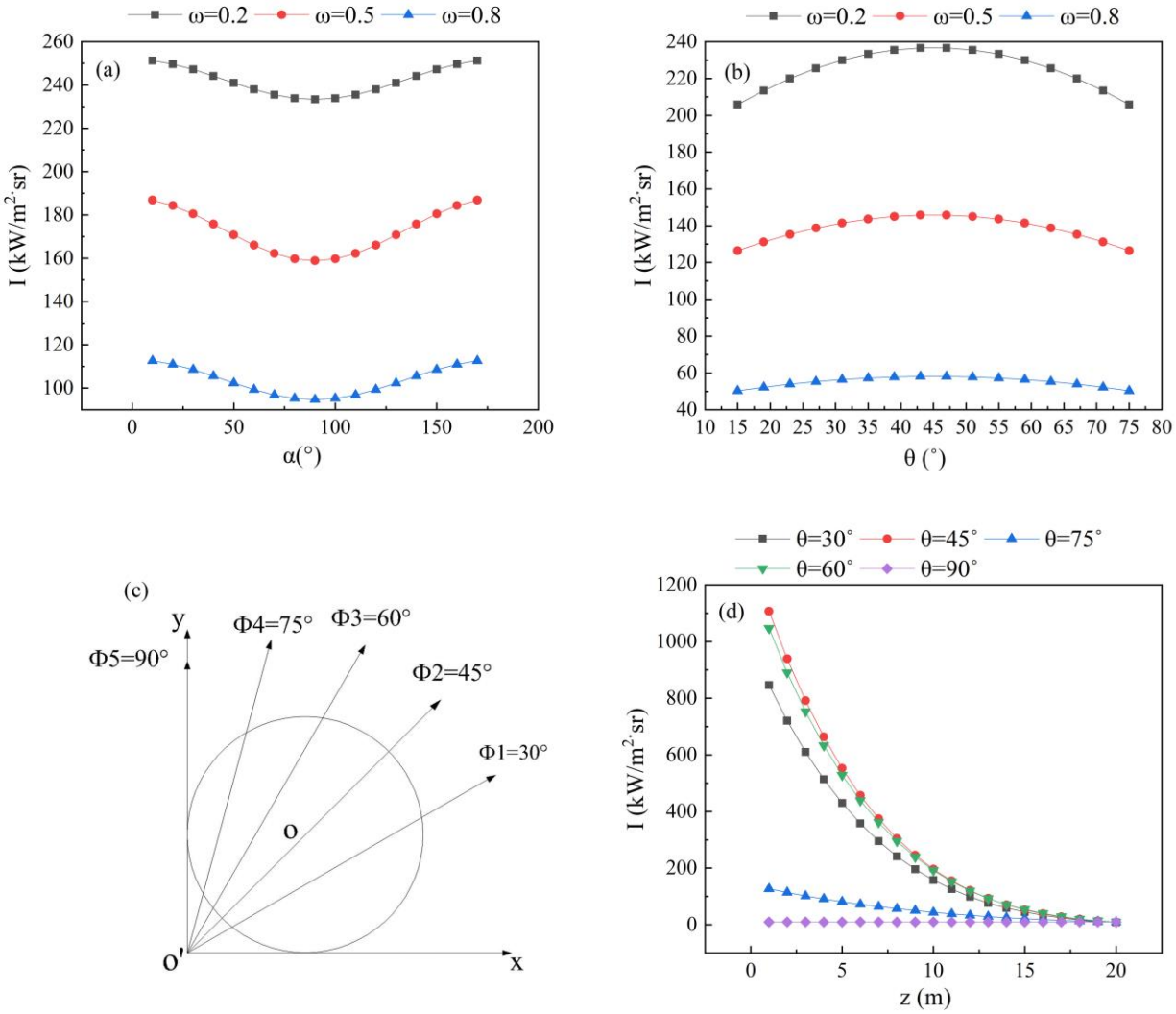

Fig. 3. (a) The radiative intensity versus polar angles under different scattering albedos, (b) The radiative intensity versus azimuthal angles under different scattering albedos, (c) The schematic of detection rays with different azimuthal angles, (d) The radiative intensities along different azimuthal angles (color online)

Fig. 4 is the radiation intensity at the interface of the two-layer composite ceramic, that is, the radiation exits from the o' point in the ceramic 1 along different incident angles $\theta = 5°, 15°, 30°, 35°$ enter the ceramic 2 and the first beam of light radiation intensity is related to the distance x from the ceramic interface.When for the model of Fig. 4, the refractive indices of the two ceramics and air are $n_1 = 0.77$, $n_2 = 0.45$, $n_3 = 1$, and the attenuation coefficient $\beta = 1\text{m}^{-1}$, and the distance of o'transverse to the interface $L_1 = 1\text{m}$, and the lateral length of the right medium $L_2 = 1.5\text{m}$.

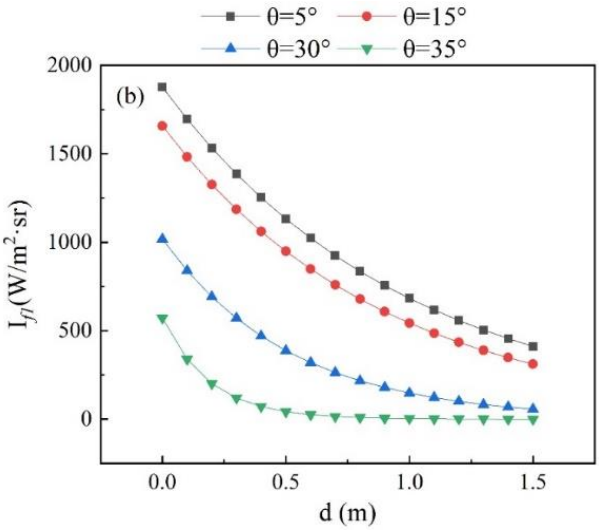

Fig. 4. The d dependent I_{fl} of the ceramic 1-ceramic 2 interface (color online)

It can be seen from Fig. 4 that the first beam of forward radiation I_{f1} entering the YAG decays exponentially with the increase of the distance d, which is consistent with the theoretical formula (11). As the radiation incident angle increases, the energy reflected by the interface increases. The transmitted energy decreases, so I_{f1} decreases with the increase of the incident angle. When the incident angle increases to close to 45°, due to the phenomenon of total reflection, the curve is no longer smooth and the radiant intensity tends to 0.

From the interface diagram of Fig. 2, one can see that the reflection and transmission occur between the ceramic 2 and air interface. Fig. 5(a) shows the first backward radiation intensity in ceramic 2 when the attenuation coefficient $\beta = 1\text{m}^{-1}$, the refractive indices of the two ceramics and air $n_1 = 0.77$, $n_2 = 0.45$, $n_3 = 1$, the lateral distance between o′ and the interface is $L_1 = 1\text{m}$, the lateral length of the medium on the right is $L_2 = 1.5\text{m}$ and the incident angle is the zenith angle $\alpha = 5°, 15°, 30°, 35°$. It can be seen that the backward radiation intensity attenuates as it approaches the ceramic 1-ceramic 2 interface. Fig. 5(b) shows the total lateral radiation intensity in ceramic 2 when the attenuation coefficient $\beta = 1\text{m}^{-1}$, the refractive indices of the two ceramics and air are $n_1 = 0.77$, $n_2 = 0.45$, $n_3 = 1$, the lateral distance between o′ and the interface is $L_1 = 1\text{m}$, the lateral length of the medium on the right is $L_2 = 1.5\text{m}$, and the incident angle is the zenith angle $\alpha = 5°, 15°, 30°, 35°$. It can be seen that the radiation attenuates in the ceramic 2 after passing through the ceramic 1-ceramic 2 interface and the smaller the incident angle, the smaller the intensity loss.

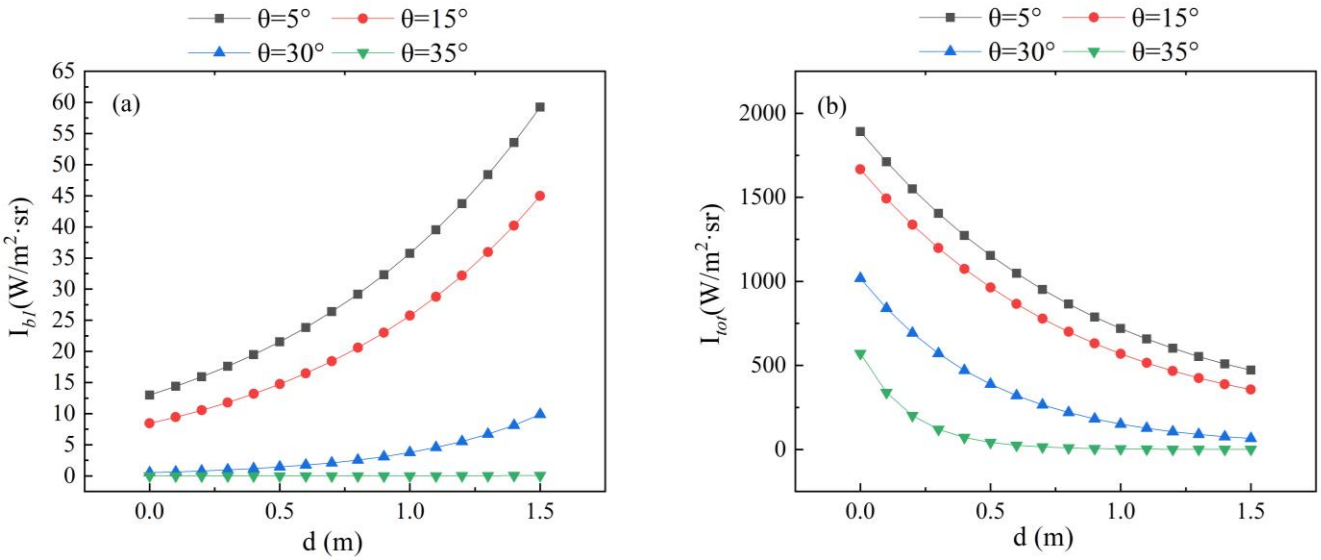

Fig. 5. (a) The d dependent I_{bl} and (b) The d dependent I_{tot} for the ceramic 2 (color online)

From Fig. 2, one can see that the radiation needs to pass through the ceramic 2-air interface after passing through the ceramic 2. We choose to study the radiation intensity of the first beam of radiation in the air and the total radiation intensity along the x-axis direction. Fig. 6(a) shows the first light intensity emitted from the ceramic 2 after entering the air interface when the attenuation coefficient $\beta = 1\text{m}^{-1}$, the refractive indices of the two ceramics and air are $n_1 = 0.77$, $n_2 = 0.45$, $n_3 = 1$, the lateral distance between o' and the interface is $L_1 = 1\text{m}$, the lateral length of the medium on the right is $L_2 = 1.5\text{m}$ and the incident angle is the zenith angle $\alpha = 5°, 15°, 30°, 35°$. It can be seen that the attenuation is almost linear in the air. Fig. 6(b) shows the total radiant light intensity transmitted from the ceramic 2-air interface when the attenuation coefficient $\beta = 1\text{m}^{-1}$, the refractive indices of the two ceramics and air are $n_1 = 0.77$, $n_2 = 0.45$, $n_3 = 1$, the lateral distance between o′ and the interface is $L_1 = 1\text{m}$, the lateral length of the medium on the right is $L_2 = 1.5\text{m}$, the incident angle is the zenith angle $\alpha = 5°, 15°, 30°, 35°$. It can be seen that the numerical value is similar to the first beam of forward radiation, the radiation intensity of the ceramic 2 is almost lost after multiple reflections and the radiation in the air is mainly dominated by the first beam of radiation.

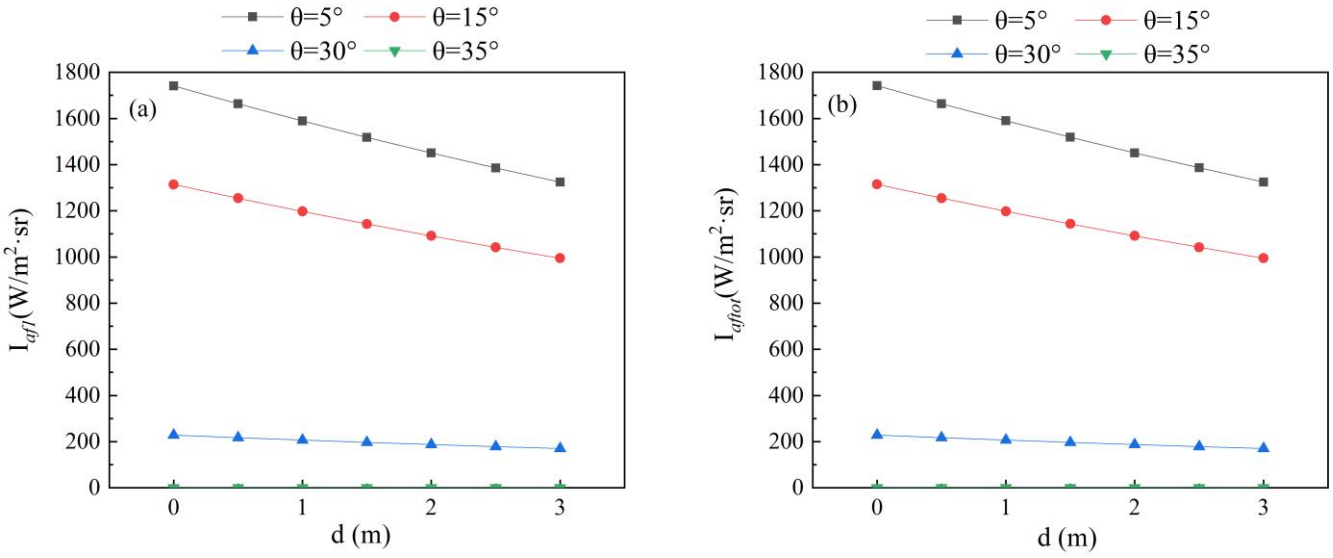

Fig. 6. The d dependent (a) I_{afl} and (b) I_{aftot} along the x-axis (color online)

4. Conclusion

In summary, we proposed a new method of calculating radiation transmission based on the radiation transfer equation for the radiation transmission problem in layered composite ceramics. We take GGAG/YAG layered composite ceramics, and calculated the transmission of radiation in the ceramic and the transmission after passing through the layered interface and the air interface. It was found that this method can obtain the numerical solution at any point in the radiation transmission process quickly and accurately. Meanwhile the radiation decays approximately exponentially in YAG after passing through the ceramics' interface. This helps us to have a better understanding of the optical radiation transmission in the medium whose equipment accuracy cannot be surveyed yet.

Acknowledgements

This work was supported by Jiangsu Natural Science Foundation for Excellent Young Scholar (BK20170101), and the Scientific Research Foundation of Nanjing University of Posts and Telecommunications (NY220011, NY2 20034), and the Anhui Province Key Laboratory of Environment-friendly Polymer Materials.

References

[1] J. J. Song, H. Yang, R. Bermejo, J. M. Qu, L. T. Hu, Y. S. Zhang, J. Am. Ceram. Soc. **102**, 3673 (2019).
[2] C. Gardner, N. S. Müller, G. Vekinis, I. C. Freestone, V. Kilikoglou, Archaeometry **62**, 935 (2020).
[3] H. Liu, J. Ma, J. Gong, J. Xu, J. Non-Cryst. Solids. **419**, 92 (2015).
[4] S. V. Reznik, P. V. Prosuntsov, K. V. Mikhailovskii, J. Eng. Phys. Thermophys. **92**, 89 (2019).
[5] C. J. Russo, M. P. Harmer, H. M. Chan, G. A. Miller, J. Am. Ceram. Soc. **75**, 3396 (1992).
[6] J. Sanghera, W. Kim, G. Villalobos, B. Shaw, C. Baker, J. Frantz, B. Sadowski, I. Aggarwal, Opt. Mater. **35**, 693 (2013).
[7] T. Yanagida, K. Watanabe, Y. Fujimoto, A. Uritani, H. Yagi, T. Yanagitani, J. Ceram. Soc. Jpn. **122**, 1016 (2014).
[8] P. Lecoq, J. Varela, Nucl. Instrum. Methods Phys. Res. Sect. A **486**, 1 (2002).
[9] G. Consolati, D. Franco, C. Jollet, A. Meregaglia, A. Minotti, S. Perasso, A. Tonazzo, Nucl. Instrum. Methods Phys. Res. Sect. A **795**, 364 (2015).
[10] H. Akitaya, M. Lye, K. Okita, M. Sato, H. Matsuo, T. Itazu, T. Uno, M. Yamaguchi, Z. Tanaka, T. Yamashita, K. S. Kawabata, M. Uemura, M. Kurita, Proc. SPIE Int. Soc. Opt. Eng. **7018**, 70183H (2014).
[11] L. J. Xu, X. Lin, Q. He, M. Worku, B. Ma, Nat. Commun. **11**, 4329 (2020).
[12] X. Chen, H. Qin, X. Wang, C. Yang, J. Jiang, H. Jiang, J. Eur. Ceram. Soc. **36**, 2587 (2016).
[13] J. Forner-Escrig, R. Mondragón, L. Hernández, R. Palma, Int. J. Mech. Sci. **188**, 105952 (2020).
[14] H. C. Hottel, E. S. Cohen, AlChE J. **4**, 3 (1958).
[15] S. Chandrasekhar, Quartely Journal of the Royal Meteorological Society **76**, 498 (1950).
[16] J. H. Jeans, Monthly Notices of the Royal Astronomical Society **78**, 28 (1917).
[17] H. P. Tan, M. Lallemand, Int. J. Heat Mass Transfer **32**, 795 (1989).
[18] C. X. Zhang, X. H. Shi, T. J. Li, Y. Yuan, F. Q. Wang, H. P. Tan, J. Quant. Spectrosc. Radiat. Transfer **245**, (2020).
[19] D. Julio, J. J. Serrano-Aguilera, P. Victor, M. Annalisa, Int. J. Multiphase Flow **146**, 103881 (2022).

[20] A. J. Banko, L. Villafañe, J. H. Kim, M. Esmaily, J. K. Eaton, J. Quant. Spectrosc. Radiat. Transfer **226**, 1 (2019).
[21] C. S. Wang, P. Y. Shen, T. M. Liou, Comput. Meth. Appl. Mech. Eng. **368**, 113200 (2020).
[22] J. Ripoll, J. Opt. Soc. Am. A: **28**, 1765 (2011).
[23] D. A. Gharbiea, Eur. Phys. J. Plus. **135**, 812 (2020).
[24] V. D. Michele, A. Morana, C. Campanella, J. Vidalot, A. Alessi, A. Boukenter, M. Cannas, P. Paillet, Y. Ouerdane, S. Girard, IEEE Trans. Nucl. Sci. **67**, 1650 (2020).
[25] M. F. Modest, Radiative Heat Transfer, 2nd Edition, New York: McGraw-Hill (2003).
[26] Y. Kuwano, S. Saito, U. Hase, J. Cryst. Growth **92**, 17 (1988).
[27] S. Yu, W. Jing, M. Tang, T. Xu, B. Kang, Ceram. Int. **45**, 19340 (2019).

*Corresponding authors: buyy@njupt.edu.cn (Bu);
xfwang@njupt.edu.cn (Wang)